

# Adaptive Fuzzy Logic Based MPPT Control for PV System under Partial Shading Condition

S.Choudhury \*<sup>‡</sup>, P.K.Rout \*

\* Department of EEE, Asst.Prof, SOA University, Bhubaneswar

(subhashree3@gmail.com, pkrou\_t\_india@yahoo.com)

<sup>‡</sup>S.Choudhury; P.K.Rout, SOA University, Bhubaneswar, Odisha, Tel: +91 8093162126,

subhashree3@gmail.com

*Received: 21.09.2015 Accepted: 05.11.2015*

**Abstract-** Partial shading causes power loss, hotspots and threatens the reliability of the Photovoltaic generation system. Moreover characteristic curves exhibit multiple peaks. Conventional MPPT techniques under this condition often fail to give optimum MPP. Focusing on the afore mentioned problem an attempt has been made to design an Adaptive Takagi-Sugeno Fuzzy Inference System based Fuzzy Logic Control MPPT. The mathematical model of PV array is simulated using in MATLAB/Simulink environment. Various case studies related to inhomogeneous insolation and temperature has been investigated. For justifying the efficacy of the proposed MPPT technique a comparative analysis has been done with two popular MPPT techniques.

**Keywords** Partial Shading, PV system, Maximum Power Point Tracking (MPPT), Takagi-Sugeno Fuzzy Interference System (TS-FIS), Fuzzy Logic Control (FLC), Total Harmonic Distortion (THD).

## 1. Introduction

Energy crisis due to rapid diminish of conventional energy sources, and increase environmental pollution has lead to strong attention towards renewable power generation employing solar, wind turbine, geothermal, biomass and hydro, to obtain an efficient and pollution free energy supply. Among all possible renewable resources photovoltaic power generation has been proved to a very powerful and promising potential [1] due to absence of investment in fuel cost, wide range of power scalability and simple implementation like on rooftops of the buildings, and low maintenance tariff after installation. Further, the PV power system has the added advantage of operating in both grid connected mode and isolation mode by integrating with proper power electronics devices [2],[3]. As per technical report of European Photovoltaic Industry Association (EPIA), capacity of photovoltaic (PV) energy is installed globally more than 31 GW in 2012, which may increase to 84 GW by 2017 according to the aggressive projections [4]. However, the major drawbacks of the PV generation system are low efficiency of energy conversion and very high installation investment cost [5],[6]. Hence, it becomes very crucial to acquire the maximum electrical energy from the available solar energy at the input PV system [7],[8]. But, PV

cell has very high non-linear operating characteristics with respect to varying temperature and insolation giving rise to suboptimal system efficiency.

However, PV system characteristic curve exhibits a optimum operating point known as maximum power point (MPP) under specific insolation and temperature condition. But, as the weather and environmental factors keep changing like insolation and surface temperature change due to partial shading, the amount of power generation by the PV system is varying and may operate at suboptimal point. As a result, the optimum values for MPP keep changing over time. So, to track the MPP at a particular operating condition, it is necessary for the PV system to develop a controller. In past few years several MPPT techniques have been proposed by various authors and some published techniques are open circuit voltage and short circuit current [9], lookup table [10], perturb and observe [11-13], incremental conductance [14-16], extremum seeking control [17] ripple correction control [18] and implementing soft computing techniques such as neural network [19],[20], genetic algorithm [21], and fuzzy logic control [22-24], etc. However, due to high nonlinear operational characteristics, tracking of maximum power point is still a

challenging task to find a optimum method for it under various practical environmental varying situations.

In general, almost all conventional and hill climbing MPPT methods work only on local optimal operating value and therefore they are implemented particularly in case of unimodal characteristic curves under uniform insolation environment. For variable insolation environment, otherwise known as for partial shading, the characteristic curves of PV system are mostly multimodal and basically represented by adoption of a bypass diode across the PV cell string. During partial shading, one PV cell in shaded region reduces the overall current of the PV module resulting high voltage across the unshaded PV cells. The high voltage produced often cause reverse bias of the shaded cell. This whole phenomenon leads to hot-spot heating in PV system and severe dissipation of heat in shaded cells could further lead to cell cracks. Hence, in order to relieve from such problem bypass diode is used in shunt. Generally, bypass diode is reverse biased, while PV cell is in forward bias under normal operating condition. Mismatch in short circuit current in series connected PV cells results in reverse bias condition. Thus, bypass diode becomes forward bias and allows the current to flow from the unshaded cells in the external circuit rather than forcing them to become forward biased. As a result, the short circuit current is reduced and hot spot heating is prevented. The bypass diode protects the PV cells of the PV module but results in generation of non-uniform currents due to device properties of the system and insolation variation or shading condition which is commonly called as mismatch. The mismatches further cause multiple peaks in the characteristics.

Hence, multiple peaks in the I vs V, P vs V and P vs I curves due to partial shading conditions give rise to several local and global maximum power point. MPPT techniques like perturb and observe and incremental conductance, do not analyse all the peaks to determine true MPP. It usually tracks the nearest optimum local maximum [25-27]. Moreover, constant perturbation by incrementing and decrementing the voltage may cause oscillations in the power of the PV system [28]. The tracking speed may also decrease and the system may become prone to wrong tracking directions.

In this paper an Adaptive Fuzzy Logic Control (FLC) based MPPT technique implementing Takagi–Sugeno (T-S) fuzzy inference system (FIS) is proposed. The proposed algorithm has better tracking ability than other conventional MPPT techniques and operates regardless the climatic variations. As Mamdani fuzzy inference system takes long processing time due to the complexity in design, Takagi–Sugeno (T-S) FIS system is implemented in the proposed MPPT technique. A PV array of 104KW has been designed using mathematical modeling for studying suitable partial shading conditions. Along with the proposed MPPT, two other well-known MPPT, i.e. Perturb and Observe (PO) and Incremental Conductance (IC) has been simulated using Sim Power System tool box in Matlab/Simulink environment. The major contributions of the paper are:

- I. Three partial shading conditions of PV array are investigated:

- A. Each module operating at the constant temperature and irradiance;
- B. Each module operating at the different irradiance pattern but same temperature;
- C. Each module operating at a different temperature as well as irradiance pattern.

- II. Takagi-Sugeno FIS based FLC is employed for MPPT
- III. Fast Fourier Transform (FFT) analysis and Total Harmonic distortion (THD) calculation of grid voltage and grid current has been performed for on grid PV system to ensure the power quality constraints
- IV. A detailed comparison has been made for the proposed technique with Incremental Conductance, and Perturb and Observe MPPT technique.

The paper has been organized as: Mathematical design approach of PV system in section 2, topology of boost converter in section 3, MPPT techniques in section 4 and simulation models and result analysis in section 5.

## 2. Mathematical design approach of PV system

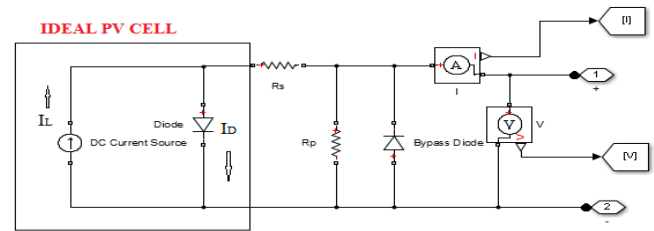


**Fig. 1.** Equivalent electrical circuit of a PV cell with a bypass diode

Fig.1 shows an electrical circuit which is equivalent of a PV cell with bypass diode. Here, the current generated due to exposure of p-n junction of the PV cell to solar irradiation is presented by a non-linear DC current source (\$I\_L\$). A diode illustrates p-n junction in the above circuit. The bypass diode protects the PV cell from overheating during partial shading. The series resistance (\$R\_s\$) represents the sheet resistance of the semiconductor body or surface. Parallel resistance (\$R\_p\$) is considered to block the leakage current from the PV cell. In this paper, \$R\_p\$ is neglected for simplification of calculation in PV mathematical model [29].

Applying Kirchhoff's current law to the equivalent electrical model of PV cell,

$$I = I_L - I_D \tag{1}$$

Where, \$I\_L\$ = Current generated by solar irradiance; \$I\_D\$ = Diode current; \$I\$ = Terminal output current of PV module. The current generated by solar irradiance is expressed as

$$I_L = (I_{L,ref} + K_i \Delta T) \frac{G}{G_{n,ref}} \tag{2}$$

Where,  $I_{L,ref}$  = Reference current generated by solar irradiance at nominal condition;  $\Delta T$  = Difference between actual temperature and nominal temperature;  $K_i$  = Temperature coefficient of maximum PV cell current ( $A^\circ K$ );  $G$  = Irradiance incident on PV module surface;  $G_{n,ref}$  = Nominal Irradiance,  $1000W/m^2$ . Diode current is calculated as

$$I_D = I_O \left[ e^{\left( \frac{V+R_S I}{\alpha V_t} \right)} - 1 \right] \tag{3}$$

Where,  $I_O$  = Diode saturation current in the absence of solar light;  $V_t$  represents PV cell thermal voltage and is expressed as

$$V_t = \frac{N_S K T}{q} \tag{4}$$

Where,  $N_S$  = Number of PV cells in series;  $K$  = Boltzmann constant =  $1.3806 \times 10^{-23}$  J/K;  $q$  = Electron charge =  $1.602 \times 10^{-19}$  C;  $T$  = Actual temperature in Kelvin;  $\alpha$  = Diode ideality constant ( $1 < \alpha < 1.5$ ).

The saturation current of the diode depending on temperature is represented as:

$$I_O = I_{O,ref} \left( \frac{T_{n,ref}}{T} \right)^3 e^{\left[ \frac{q E_g}{\alpha K} \left( \frac{1}{T_{n,ref}} - \frac{1}{T} \right) \right]} \tag{5}$$

Where,  $T_{n,ref}$  = Nominal temperature  $I_{O,ref}$  = Saturation current of diode at nominal condition;  $E_g$  = Band gap energy. The saturation current is expressed as

$$I_{O,ref} = \frac{I_{SC,ref}}{e^{\left( \frac{V_{OC,ref}}{\alpha V_{t,ref}} \right)} - 1} \tag{6}$$

Where,  $V_{OC,ref}$ ,  $I_{SC,ref}$  and  $V_{t,ref}$  are open circuit voltage, short circuit current and thermal voltage nominal values of PV module respectively. The above evaluated parameters represent a single PV cell at nominal irradiance and temperature. So to describe I versus V, P versus I and P versus V characteristic curves for the whole module having cells in series and parallel configuration, the parameters are scaled as:

$$I_{L,Total} = N_p * I_L \tag{7}$$

$$I_{O,Total} = N_p * I_O \tag{8}$$

$$R_{S,Total} = \frac{N_S}{N_p} * R_s \tag{9}$$

Where  $N_S$  and  $N_p$  are the number of PV cells in series and parallel respectively. Therefore,

$$I_{Total} = N_p * I \tag{10}$$

$$V_{Total} = N_S * V \tag{11}$$

The mathematical PV modeling is implemented in MATLAB/Simulink software referring the above mentioned equations and the value of the mentioned parameters are presented in appendix.

### 3. DC-DC boost converter topology

The optimal operating point of PV system depends upon the load curve which is represented as a straight line with slope

$$I = \frac{1}{R} * V$$

and the P-V curve. Hence, the maximum power point that can be delivered to the load depends upon the optimal value of the resistive load. But, if the load varies the output power also varies depending upon the value of R load [30]. So, to overcome the undesired PV power fluctuation, DC-DC boost converter topology is integrated between PV module and load so as to maximize the power transfer from PV system to load. Also it insures adaptation of the impedance by synchronizing load impedance with fluctuating PV power [31].

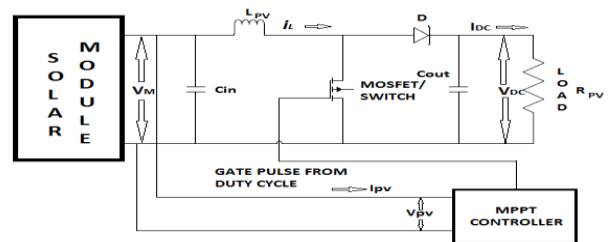


Fig. 2. DC-DC boost converter topology

The DC-DC boost converter topology is shown in Fig.2. It basically has two conduction modes, i.e. continuous conduction mode for efficient conversion of power and discontinuous conduction mode for low power operation or stand by operation. The model can be mathematically expressed as:

$$\begin{bmatrix} V_m \\ i_{dc} \end{bmatrix} = m \begin{bmatrix} V_{DC} \\ i_L \end{bmatrix} \tag{12}$$

Where,  $m = 1 - D$ ;  $D$  = duty cycle fed to the converter switch;  $i_L$  and  $i_{dc}$  are the instantaneous values of  $I_L$  and  $I_{dc}$  respectively.  $V_m$  is the voltage across the PV array and  $V_{DC}$  is the voltage across the capacitor of DC-DC boost converter.  $D$  is calculated as:

$$D = \frac{t_{on}}{T} = t_{on} * f_s \tag{13}$$

Where,  $f_s$  is the switching frequency of the MOSFET/Switch of the converter;  $T$  is the total time of one cycle;  $t_{on}$  is the turn on time of one cycle.

The DC-DC boost converter has two operation modes. In Mode I, MOSFET/Switch is turned ON and current from PV module circulates through the inductor ( $L_{PV}$ ) and MOSFET. In Mode II, MOSFET/Switch is turned OFF and the current circulates through the inductor ( $L_{PV}$ ), the diode (D), the capacitor ( $C_{out}$ ) and the R load as represented in Fig.2. Inductor ( $L_{PV}$ ) stores energy in mode one and dissipates the energy back to the circuit in mode two. As a result, the R load constantly receives power even when switch is turned off and as a result output voltage is boosted up.

**4. MPPT Techniques**

*4.1. Modified Perturb and Observe (MPO) MPPT Technique*

Under rapid irradiance changes the conventional P&O method may become unstable and the step-size has a strong impact on the tracking performance. In this part, a coarse explanation to the relationship between step-size and MPPT performance is presented and is so termed as modified P&O technique.

In this MPPT technique, consistent perturbation of current and voltage of PV system is performed. If an increase in power is tracked i.e.  $\Delta P > 0$ , then the subsequent perturbation remains in particular direction so as to reach maximum power point (MPP). But, if a decrease in power is tracked i.e.  $\Delta P < 0$ , then the perturbation direction is reversed [32]. Fig.3 presents the algorithm for MPO MPPT algorithm.

The proposed modified MPPT method can be described as the following: If  $|\Delta P| > P_{th}$ , the step-size is  $V_{stp1}$ ; and it could rapidly track the MPP; when  $|\Delta P| \leq P_{th}$ , the step-size becomes  $V_{stp2}$  (smaller) and the proposed method should be able to offer a more accurate tracking response.

Using the above step-sizes may also lead to more power losses if the solar irradiance is very low. To counteract the above problem, a power ratio,  $P_r$ , is added into this MPPT control algorithm as also shown in Fig. 3. This power ratio is

defined as the following:  $P_r \triangleq \frac{P_{ins}}{P_{mn}}$  where  $P_{ins}$  is the

instantaneous power under different solar irradiance conditions and  $P_{mn}$  is the nominal maximum power under standard test condition (solar irradiance: 1000 W/m<sup>2</sup>, ambient temperature: 25 °C, air mass of 1.5 solar spectral irradiance distribution).

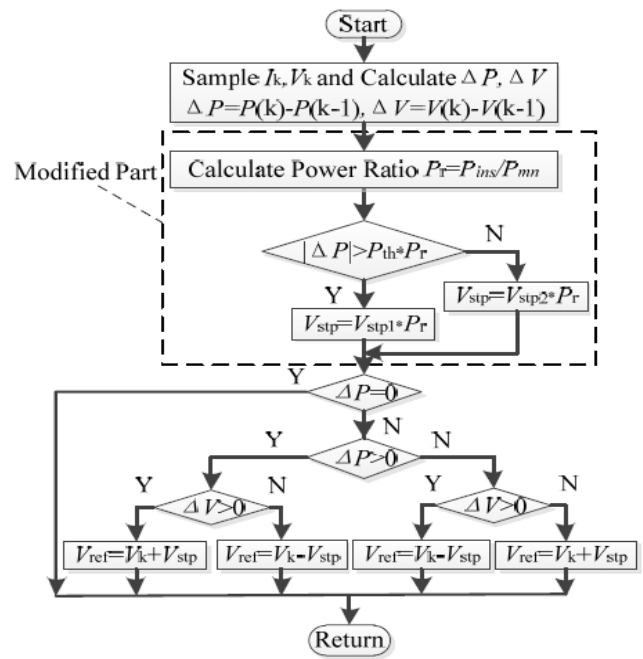


**Fig.3. MPO MPPT algorithm**

*4.2. Modified Incremental Conductance (MIC) MPPT Technique:*

MIC MPPT technique acquires derivative of conductance i.e.  $\frac{dI}{dV}$  to detect the optimal operating point location with respect to MPP. The slope of the tangent of P-V characteristic curve of PV power and voltage obtained at MPP is zero. The tangent slope will be positive, if its location is on left hand side of the maximum power point (MPP) and the tangent slope has a negative value if it is obtained on right hand side of MPP [33]. The calculation of slope of tangent is given by:

$$\frac{\Delta P}{\Delta V} = \frac{\Delta(VI)}{\Delta V} = I + V \frac{\Delta I}{\Delta V} \tag{14}$$

Fig.4. illustrates the algorithm for MIC MPPT technique [34]. The algorithm evaluates  $\frac{I}{V}$  and  $\frac{\Delta I}{\Delta V}$  at every instant so as to deduce the direction of the perturbation favourably towards the MPP. The perturbation with the help of controller generates duty cycle which provides gate pulse to the switch of DC-DC boost converter. The process of incrementing and decrementing performed repeatedly in MPO MPPT and MIC MPPT to track MPP result in system oscillation about the MPP and also further causing power loss in the system. Moreover, it is difficult to choose optimum step size taking into account both tracking accuracy and speed of response for both the above methods. Apart from that, even if the MPP is reached, the sustained oscillations occur around the optimum solution point.



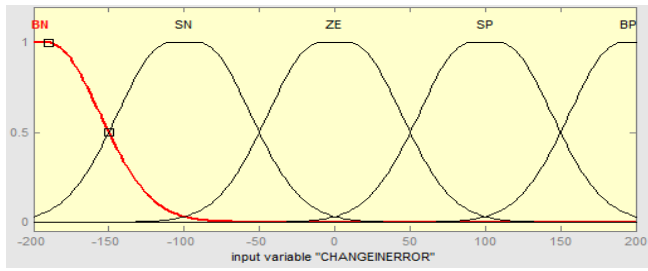


Figure 6b. Membership function of change in error

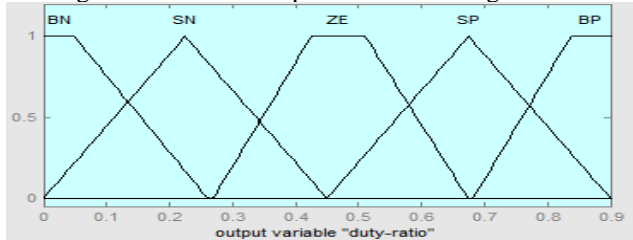


Figure 6c. Membership function of duty ratio

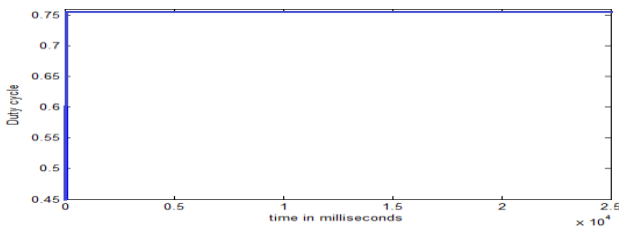


Figure 6d. Duty cycle of FLC MPPT controller

4.3.2. Inference engine:

Inference engine fuzzifies the input crisp values in order to determine fuzzy output values by applying the rules from fuzzy rule base. In this paper Takagi–Sugeno (T-S) fuzzy inference system (FIS) is proposed. The fuzzy output, i.e. duty is shown in Fig.7. Table 1 shows fuzzy rule base table. The table provides 25 fuzzy control rules for determination of duty ratio as fuzzy output. Further, the 25 fuzzy control rules are presented in three dimensional surfaces as shown in Fig.8. In this paper, the inference engine in FLC uses Max-min fuzzy composition to obtain output. The rule viewer of the Takagi-Sugeno based FLC MPPT technique is shown in Fig.9.

| de | BN             | SN              | ZE              | SP              | BP              |
|----|----------------|-----------------|-----------------|-----------------|-----------------|
| BN | Y <sub>1</sub> | Y <sub>6</sub>  | Y <sub>11</sub> | Y <sub>16</sub> | Y <sub>21</sub> |
| SN | Y <sub>2</sub> | Y <sub>7</sub>  | Y <sub>12</sub> | Y <sub>17</sub> | Y <sub>22</sub> |
| ZE | Y <sub>3</sub> | Y <sub>8</sub>  | Y <sub>13</sub> | Y <sub>18</sub> | Y <sub>23</sub> |
| SP | Y <sub>4</sub> | Y <sub>9</sub>  | Y <sub>14</sub> | Y <sub>19</sub> | Y <sub>24</sub> |
| BP | Y <sub>5</sub> | Y <sub>10</sub> | Y <sub>15</sub> | Y <sub>20</sub> | Y <sub>25</sub> |

Table.1 Fuzzy rule base of 25 control rules

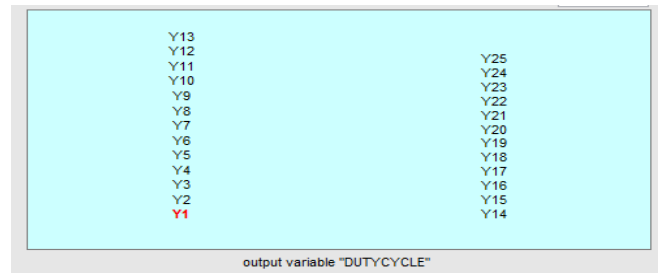


Figure 7. Membership function of duty ratio

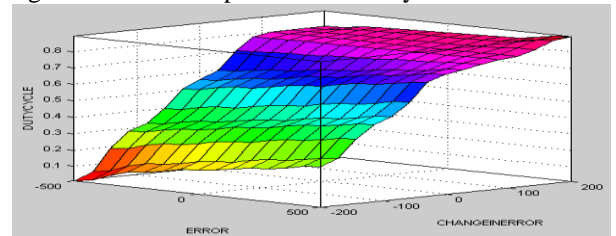


Figure 8. 3-D surface view of 25 control rules of T-S FIS based FLC

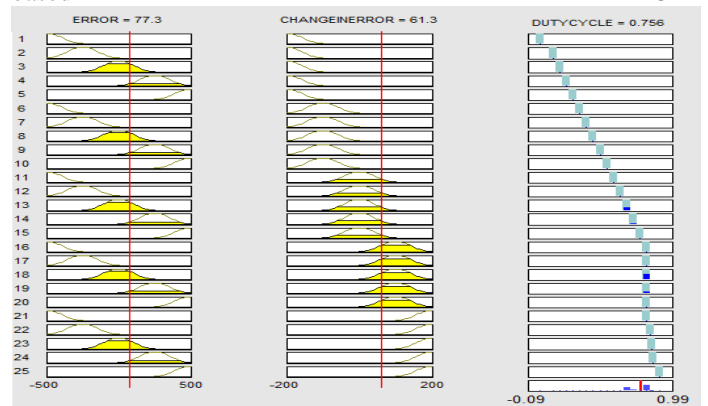


Figure 9. MATLAB/Simulink window of Rule viewer of T-S FIS based FLC

4.3.3. Defuzzification interface:

In the defuzzification process the duty ratio obtained is further scaled and fed to DC-DC boost converter to control the gate pulse of switch/IGBT/MOSFET. Defuzzification interface basically follows determination of centre of gravity or centre of area of the output fuzzy set and the centre of gravity, dD is calculated by:

$$dD = \frac{\sum_{i=1}^m \mu(dD_i) \cdot dD_i}{\sum_{i=1}^m \mu(dD_i)} \quad (17)$$

After Defuzzification the duty ratio is further scaled as before and fed to DC-DC boost converter as per the equation given below:

$$\text{Duty cycle, } D(t) = D(t - 1) + k_d dD(i) \quad (18)$$

And  $k_d$  is the gain for scaling the duty cycle which may vary from 0.1 to 0.5.

**2. Simulation models and result analysis**

Mathematical model of a PV array of 104KW has been designed using Sim-Power-System tool box in Matlab/Simulink environment as described in section 2 using the value of the parameters as given in appendix. The I vs V, P vs V and P vs I characteristic curves have been plotted where V, I and P are voltage, current and power of the PV array. The Fig.10 shows 5 PV modules connected in series to form a PV array that produce 104KW power at nominal condition of 1000W/m<sup>2</sup> irradiance and 25°C temperature. The arrangement of the model is coordinated as such in order to incorporate the study of partial shading condition.

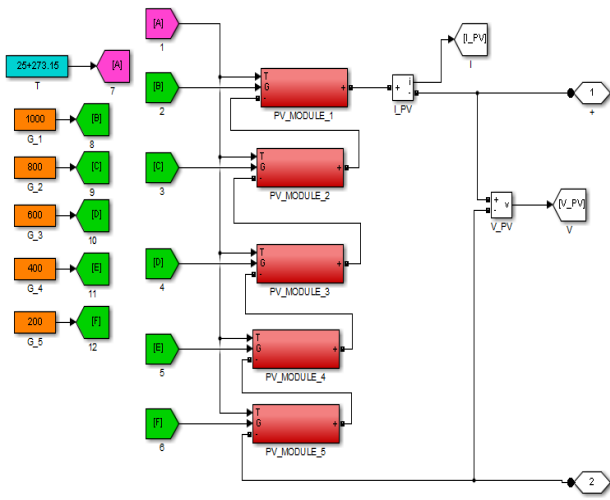


Figure 10. 5 PV modules connected in series to form a PV array for studying partial shading condition

In this paper three partial shading conditions of PV array has been investigated:

- I. Each module operating at the constant temperature and irradiance;
- II. Each module operating at the different irradiance pattern but same temperature;
- III. Each module operating at a different temperature as well as irradiance pattern.

**Case I: Comparison of parameter of PV system at nominal condition, partial shading condition and partial shading condition without using bypass diode**

Fig.11.a,b,c shows comparison of I-V, P-V and P-I characteristic curves of the PV system respectively for nominal condition (i.e. 1000W/m<sup>2</sup> irradiance and 25°C temperature), partial shading condition employing the irradiance pattern shown in Fig.10 (i.e. 1000W/m<sup>2</sup>, 800W/m<sup>2</sup>, 600W/m<sup>2</sup>, 400W/m<sup>2</sup>, 200W/m<sup>2</sup>) and partial shading condition without using bypass diode with same irradiance pattern. In Fig.11.a,b,c, curves exhibits the single MPP for nominal condition and without using bypass diode whereas exhibits several local MPP and one global MPP during partial shading condition. Fig.11.d,e,f shows comparison of current, voltage and power characteristics of the PV system at nominal condition, partial shading condition

and partial shading condition without using bypass diode respectively.

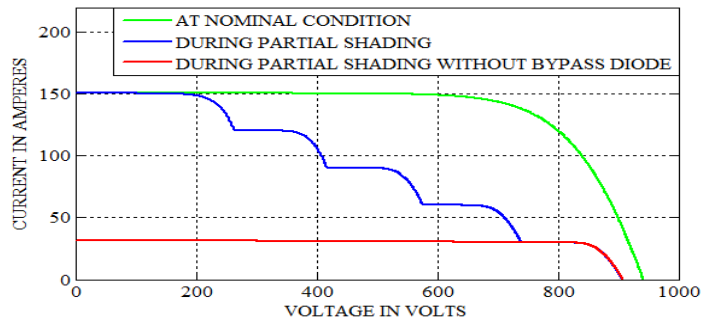


Figure 11a. V-I characteristics of PV system using bypass diode

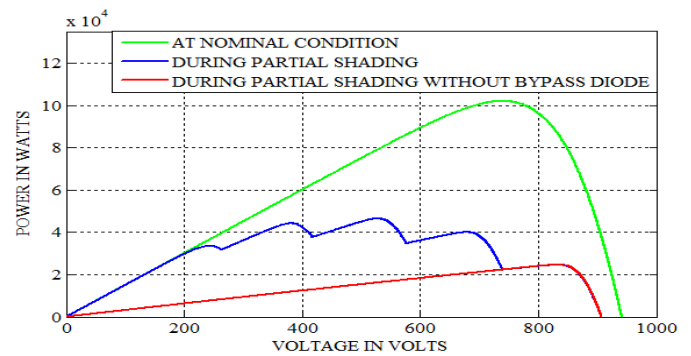


Figure 11b. P-V characteristics of PV system

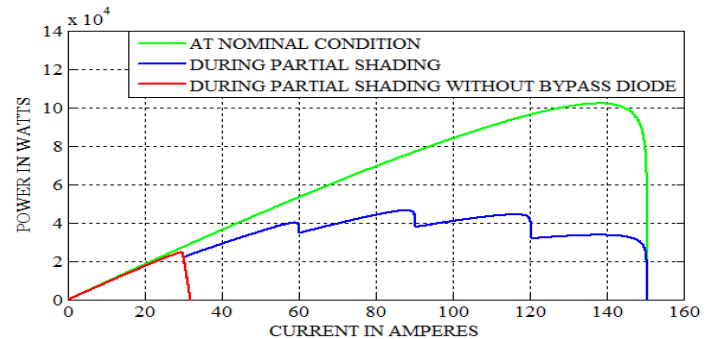


Figure 11c. P-I characteristics of PV system

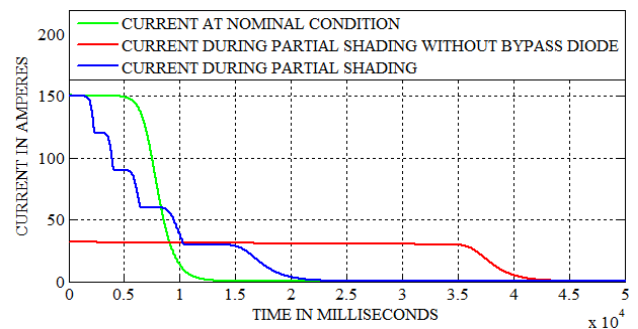


Figure 11d. Comparison of current characteristics

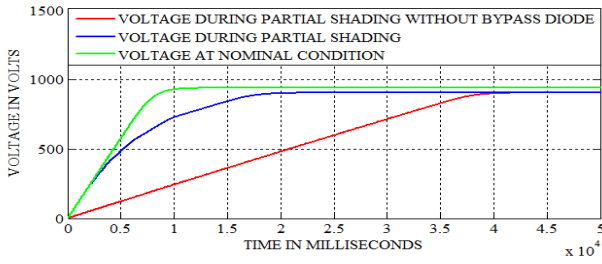


Figure 11e. Comparison of voltage characteristics

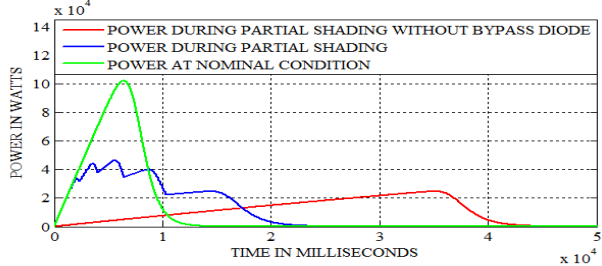


Figure 11f. Comparison of power characteristics  
**CaseII. Comparison of parameter of PV system at constant temperature of 25°C and different irradiance pattern**

The three irradiance pattern considered for study of partial shading condition at constant temperature and variable irradiance are given below:

PATTERN 1: 1000 W/m<sup>2</sup>, 850 W/m<sup>2</sup>, 750W/m<sup>2</sup>, 550W/m<sup>2</sup>, and 450W/m<sup>2</sup>

PATTERN 2: 950W/m<sup>2</sup>, 750W/m<sup>2</sup>, 450W/m<sup>2</sup>, 300W/m<sup>2</sup>, and 200 W/m<sup>2</sup>

PATTERN3: 850W/m<sup>2</sup>, 500W/m<sup>2</sup>, 350W/m<sup>2</sup>, 250W/m<sup>2</sup> and 100W/m<sup>2</sup>

Fig.12.a,b,c shows comparison of I-V, P-V and P-I characteristic curves of the PV system respectively, at constant temperature of 25°C and different irradiance pattern as mentioned above. It can be concluded from the figure that the current of PV system depends upon the irradiance change. As the irradiance or insolation increases, the PV output current increases. PV modules acquiring greater irradiance exhibits global MPP due to greater current flowing through the string and the multiple local MPPs are the result of irradiance fluctuation due to the irradiance pattern considered. Fig.12.d,e,f shows comparison of current, voltage and power characteristics of the PV system at constant temperature of 25°C and different irradiance pattern.

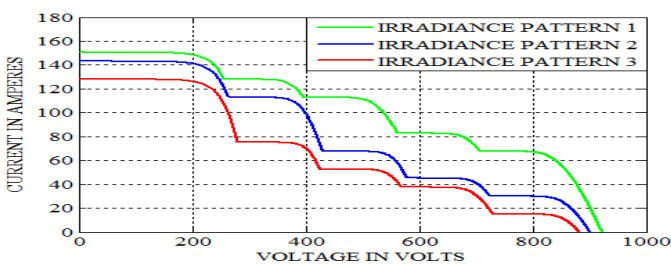


Figure 12a. V-I characteristics at constant temperature of 25°C and different irradiance pattern

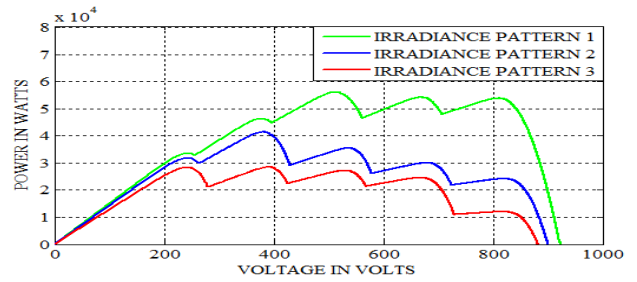


Figure 12b. P-V characteristics at constant temperature of 25°C and different irradiance pattern

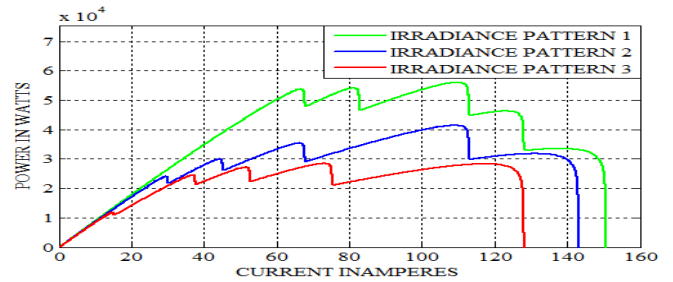


Figure 12c. P-I characteristics at constant temperature of 25°C and different irradiance pattern

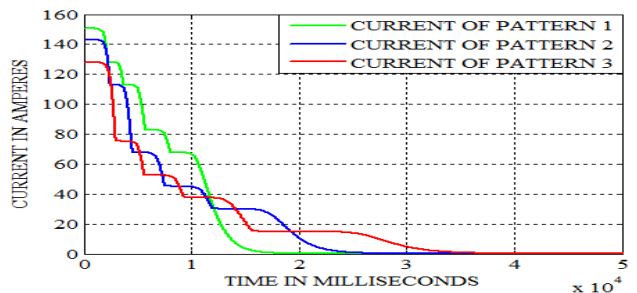


Figure 12d. Comparison of current characteristics at constant temperature of 25°C and different irradiance pattern

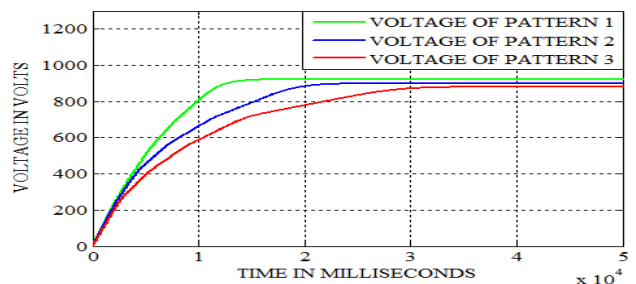


Figure 12e. Comparison of voltage characteristics at constant temperature of 25°C and different irradiance pattern

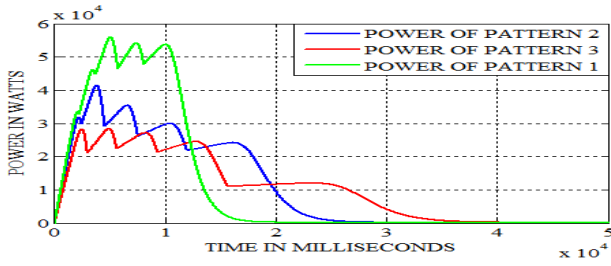


Figure 12f. Comparison of power characteristics at constant temperature of 25°C and different irradiance pattern  
**Case.III. Comparison of parameter of PV system at different temperature and irradiance pattern**

Fig.13.a,b,c shows comparison of I vs V, P vs V and P vs I characteristic curves of the PV system respectively at different temperature and irradiance pattern. The simulation is tested keeping constant irradiance pattern i.e. 1000W/m<sup>2</sup>, 800W/m<sup>2</sup>, 600W/m<sup>2</sup>, 400W/m<sup>2</sup>, 200W/m<sup>2</sup> and taking different temperature i.e., 30°C, 100°C, 170°C. It can be concluded from the figure that the voltage of PV system depends upon the temperature change. As the temperature decreases, the PV output voltage falls. PV array at lesser temperature exhibits higher numerical value of global MPP due to higher voltage across the string and the multiple local MPPs are the result of irradiance fluctuation due to the irradiance pattern considered and change in temperature. Fig.13.d,e,f shows comparison of current, voltage and power characteristics of the PV system at different temperature and irradiance pattern.

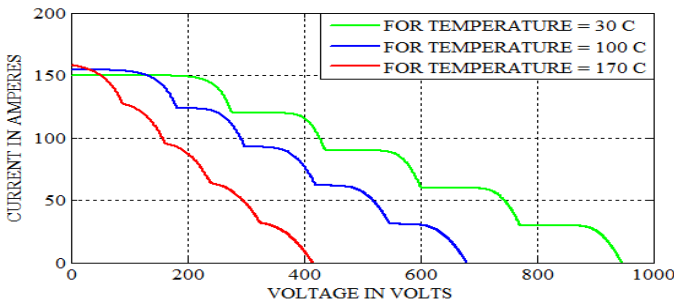


Figure 13a. Comparison of V-I characteristics at different temperature and irradiance pattern

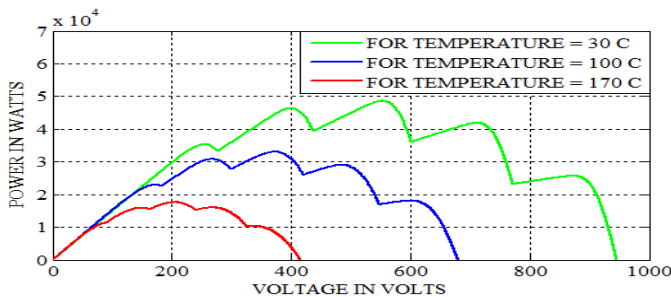


Figure 13b. Comparison of P-V characteristics at different temperature and irradiance pattern

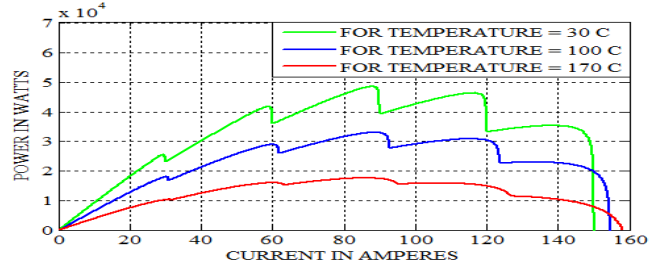


Figure 13c. Comparison of P-I characteristics at different temperature and irradiance pattern

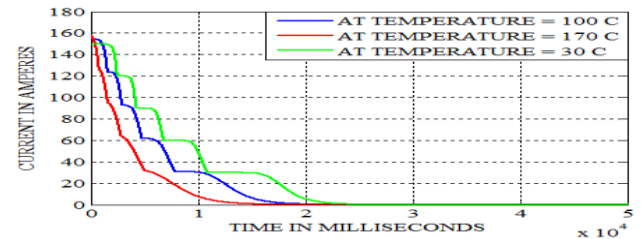


Figure 13d. Comparison of current characteristics at different temperature and irradiance pattern

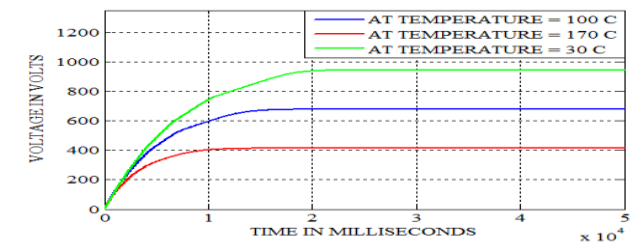


Figure 13e. Comparison of voltage characteristics at different temperature and irradiance pattern

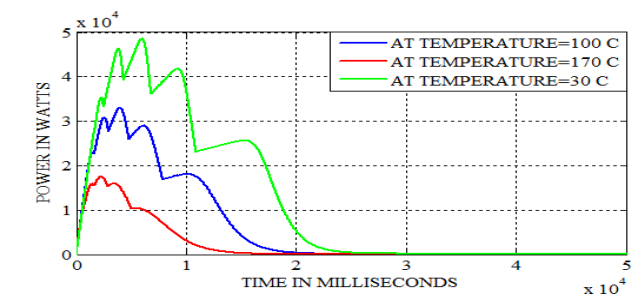


Figure 13f. Comparison of power characteristics at different temperature and irradiance pattern

**Case.IV. Comparison of voltage,current and power of PV system with different MPPT techniques in grid connected condition**

Fig.14 shows a 104KW PV power generation system mathematically designed in MATLAB/Simulink software. The PV system consists of 5 PV modules in series with different insolation values i.e. 1000W/m<sup>2</sup>, 800W/m<sup>2</sup>, 600W/m<sup>2</sup>, 400W/m<sup>2</sup> and 200W/m<sup>2</sup> and 25°C temperature. The PV system is connected to the inverter and three phase grid via DC-DC boost converter. The PV array generates 104 kilo-watts at nominal temperature and

irradiance. Performance of three MPPT techniques are compared in this paper i.e. PO MPPT, IC MPPT and T-S FIS based FLC MPPT techniques. The MPPT techniques employed control the duty ratio of the boost converter.

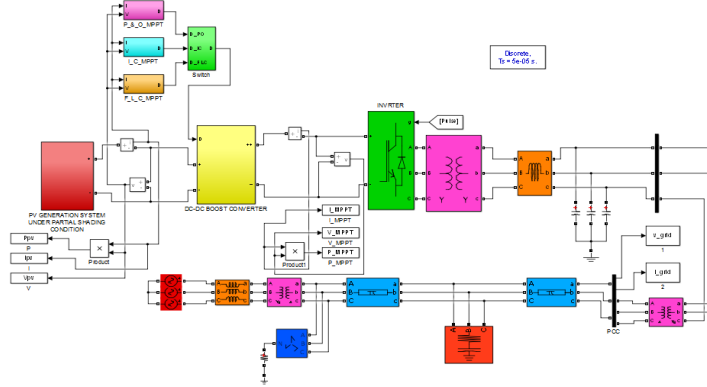


Figure 14. MATLAB/Simulink model of on grid PV system

Fig.15.a,b,c shows comparison of current, voltage and power characteristics of on grid PV system employing different MPPT techniques w.r.t time. Fig.15.a. shows the current comparison of three MPPT techniques with PV system current. The output current obtained across the boost converter implementing MPO MPPT technique is 5.62% greater than the PV output current, whereas the MIC MPPT techniques provides an increase of 4.61% than MPO MPPT technique. But, the proposed MPPT technique has 11.86% greater current value than MIC MPPT and 23.59% than PV output current. Hence, the proposed MPPT technique proves to have greater effectiveness, tracking ability and speed in comparison with MIC and MPO MPPT techniques. Similarly, in Fig.15.b, the voltage comparison has been studied where implementation of MPO MPPT technique increases the output voltage by 0.82% and MIC MPPT technique provides an increase of 4.76% w.r.t MPO MPPT technique. But, T-S FIS FLC MPPT leads MIC MPPT technique by 4.54% and PV output voltage by an overall increase of 10.42%. Fig.15.c shows power comparison of MPO, MIC and proposed fuzzy MPPT technique w.r.t PV system output power. MPO MPPT technique boosts the output power of PV by 2.59% whereas MIC MPPT technique enhances PV power by 8.12%. But, the proposed MPPT technique boosts the power by 10.01% w.r.t MIC MPPT and 18.92% w.r.t PV output power, proving better efficiency than MIC and MPO MPPT technique.

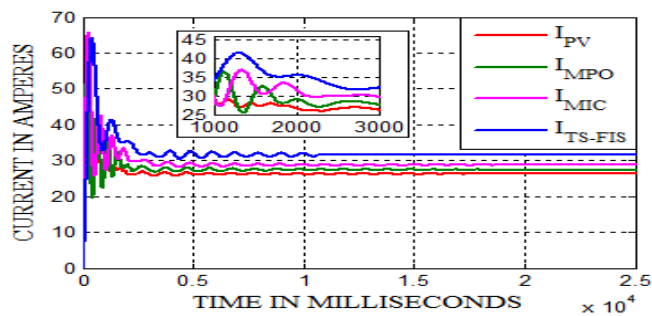


Figure 15a. Comparison of current characteristics of on grid PV system employing different MPPT techniques w.r.t time

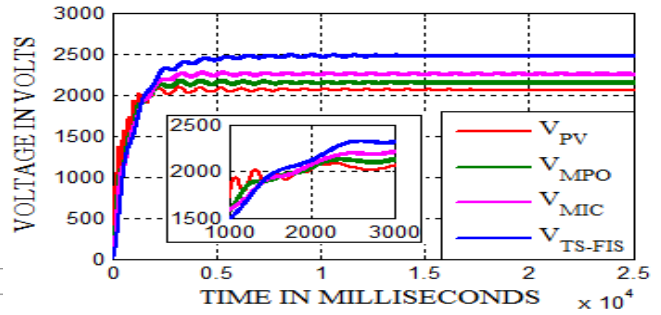


Figure 15b. Comparison of voltage characteristics of on grid PV system employing different MPPT techniques w.r.t time

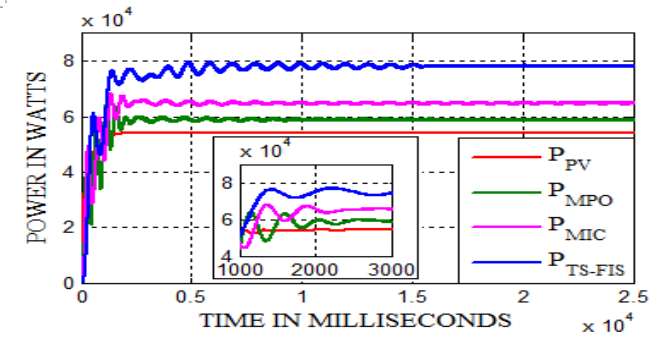


Figure 15c. Comparison of power characteristics of on grid PV system employing different MPPT techniques w.r.t time

Fig.16. and Fig.17. shows the grid voltage and current at PCC where PV system is integrated to the grid. Fig.18.a and b shows the Fast Fourier Transform (FFT) analysis of grid voltage and current. The total harmonic distortion (THD) for maximum frequency of 1000Hz is found out to be 3.29% for grid voltage and 4.61% for grid current.

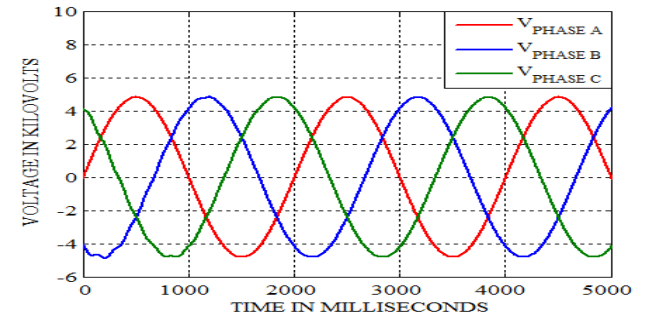


Figure 16. Grid voltage at PCC

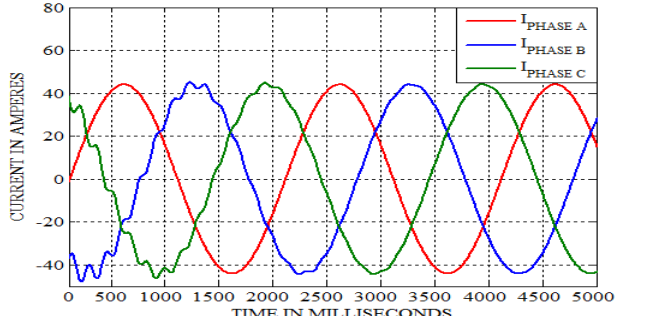


Figure 17. Grid current at PCC

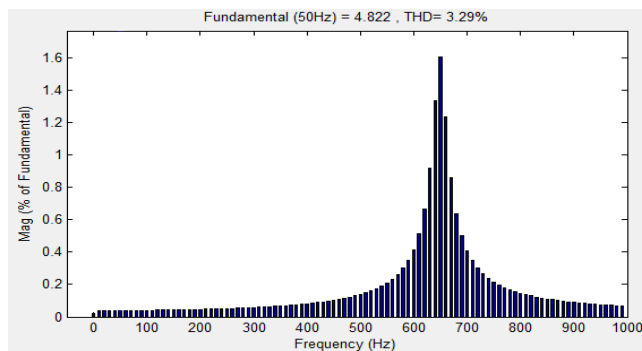


Figure 18. FFT analysis of grid voltage

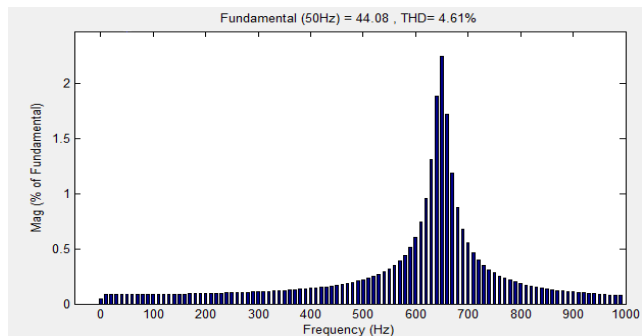


Figure 19. FFT analysis of grid current

### 3. Conclusion

In this paper a novel adaptive fuzzy logic based MPPT technique is suggested and to justify its better performance the results are compared with two other proved techniques. All the techniques are implemented on a grid connected PV system as shown in the simulation model to study their individual efficiency and response for tracking the maximum power point under various partial shading conditions. The proposed fuzzy logic based MPPT controller has been proved to be better MPPT technique as compare to other conventional MPPT techniques in terms of efficiency and tracking ability and harmonic reduction. It has better speed of response towards the PV system even without the knowledge of the actual model and the optimal operating point does not oscillate around the MPP. Further the FFT analysis of grid voltage and current indicates that the THD values are well within the prescribed IEEE standard.

### Appendix:

Parameters involved in design of mathematical model of PV  
 $N_s = 54$ ;  $G_{n,ref} = 1000W/m^2$ ;  $T_{n,ref} = 25^\circ C$ ;  $I_m = 7.61$ ;  $V_m = 36.3V$ ;  $P_m = 104KW$ ;  $V_{OC,ref} = 32.9V$ ;  $I_{SC,ref} = 68.21A$ ;  
 $R_p = 415.405\Omega$ ,  $R_s = 0.221\Omega$ ,  $K_i = 0.0032A/^{\circ}K$ ,  $K_v = 0.073V/^{\circ}K$

Parameters taken for implementation of the dc-dc boost converter topology in the simulated model of are:

$$L_{PV} = 290\mu H; C_{in} = 250\mu F \text{ and } C_{out} = 330\mu F.$$

Parameters taken for grid:

$$4.4KV, 50Hz, X/R=7$$

### References

- [1] Doty, G., McCree, D., Doty, J., Doty, F., (2010) 'Deployment prospects for proposed sustainable energy alternatives in 2020', In: Proceedings of the ASME 2010 4th International Conference on Energy Sustainability, pp. 171–182.
- [2] Figueres, E., Garcera, G., Sandia, J., Gonzalez, E. F., Rubio, J.C., (2009) 'Sensitivity study of the dynamics of three-phase photovoltaic inverters with an LCL grid filter', IEEE Trans Ind Electron Mar. 2009;56(3):706e17.
- [3] Datta, M., Senju, T., Yona, A., Funabashi, T., Chul, H. K, (2009) 'A coordinated control method for leveling PV output power fluctuations of PV-diesel hybrid systems connected to isolated power utility', IEEE Trans Energy Convers Mar.2009;24(1):153e62.
- [4] Gaëtan, M., Marie, L., Manoël, R., (2013) 'Theologitis IT, Myrto P. Global Market Out look For Photovoltaics 2013-2017', In: Proceedings of the European Photovoltaic Industry Association, Belgium; 2013.p.1–60.
- [5] Moradi, M.H., Reza Tousi, S.M., Nemati, M., SaadatBasir, N., Shalavi, N., (2013) 'A robust hybrid method for maximum power point tracking in photovoltaic systems', Sol. Energy 94, 266–276.
- [6] Tey, K.S., Mekhilef, S., (2014) 'Modified incremental conductance MPPT algorithm to mitigate inaccurate responses under fast-changing solar irradiation level', Sol. Energy 101, 333–342.
- [7] Maki, A., Valkealahti, S., (2012) 'Power losses in long string and parallel-connected short strings of series-connected silicon-based photovoltaic modules due to partial shading conditions', IEEE Trans Energy Convers 2012;27:173e83.
- [8] Martinez, M.F., Munoz, J., Lorenzo, E., (2010) 'Experimental model to estimate shading losses on PV arrays', Sol Energy Mater Sol Cells 2010; 94:2298e303.
- [9] Fangrui, L., Shanxu, D., Fei, L., Bangyin, L., Yong, K. (2008) 'A variable step size INC MPPT method for PV systems', IEEE Transactions on Industrial Electronics, Vol.:55, No.:7, pp: 2622–2628.
- [10] Liu, C.X., and Liu, L.Q., (2009) 'Research into maximum power point tracking method of photovoltaic generate system', in Proc. 2009 Int. Workshop on Intelligent Systems and Applications (ISA 2009), 2009.
- [11] Petrone, G., Spagnuolo, G., Vitelli, M. (2011) 'A multivariable perturb and observe maximum power point tracking technique applied to a single-stage photovoltaic inverter', IEEE Transactions on Industrial Electronics, Vol.:58, pp:76–84.
- [12] Yang, B., Li, W., Zhao, Y., He, X. (2010) 'Design and analysis of a grid connected photovoltaic power system', IEEE Transactions on Power Electronics Vol.:25, pp:992–1000.
- [13] Patel, H., Agarwal, V. (2008) 'Maximum power point tracking scheme for PV systems operating under

- partially shaded conditions', IEEE Trans Ind Electron April 2008;55(4).
- [14] Ji, Y.H., Jung, D.Y., Kim, J.G., Kim, J.H., Lee, T.W., Won, C.Y., (2011) 'A real maximum power point tracking method for mismatching compensation in PV array under partially shaded conditions', IEEE Trans Power Electron April 2011;26(4).
- [15] Kjaer, S.B., (2012) 'Evaluation of the "hill climbing" and the "incremental conductance" maximum power point trackers for photovoltaic power systems', IEEE Transactions on Energy Conversion Vol.:27, pp:922–929.
- [16] Kish, G.J., Lee, J.J., Lehn, P.W., (2012) 'Modelling and control of photovoltaic panels utilising the incremental conductance method for maximum power point tracking', IET Renewable Power Generation, Vol.: 6, pp: 259–266.
- [17] Lei, P., Li, Y., Chen, Q., and Seem, J. E., (2010) 'Extremum seeking control based integration of MPPT and degradation detection for photovoltaic arrays', in *Proc. 2010 Amer. Control Conf.*, submitted for publication.
- [18] Eram, T., Kimball, J.W., Krein, P.T., Chapman, P.L., Midya, P., (2006) 'Dynamic maximum power point tracking of photovoltaic arrays using ripple correlation control', IEEE Trans Power Electron Sep. 2006;21(5):1282e91.
- [19] Liu, Y.-H., Liu, C.-L., Huang, J.-W., Chen, J.-H. (2013), 'Neural-network based maximum power point tracking methods for photovoltaic systems operating under fast changing environments', Solar Energy Vol.:89, pp:42–53.
- [20] Salah, B.C., Ouali, M., (2011) 'Comparison of fuzzy logic and neural network in maximum power point tracker for PV systems', Electric Power Systems Research, Vol.: 81, pp: 43–50.
- [21] Miyatake, M., Toriumi, F., Endo, T., Fujii, N., (2007) 'A novel MPPT controlling several converters connected to PV arrays with PSO technique', In: Proceedings of power electronics application European conference 2007. p. 1e10.
- [22] Rajesh, R., Mabel, M.C., (2014) 'Efficiency analysis of a multi-fuzzy logic controller for the determination of operating points in a PV system', Solar Energy Vol.: 99, pp:77–87.
- [23] Messai, A., Mellit, A., Guessoum, A., Kalogirou, S.A. (2011) 'Maximum power point tracking using a GA optimized fuzzy logic controller and its FPGA implementation', Solar Energy Vol.:85, pp:265–277.
- [24] Chiu, C.-S. (2010) 'T-S fuzzy maximum power point tracking control of solar power generation systems', IEEE Transactions on Energy Conversion, Vol.: 25, pp: 1123–1132.
- [25] Qi, J., Zhang, Y., Chen, Y., (2014) 'Modeling and maximum power point tracking (MPPT) method for PV array under partial shade conditions', Renew. Energy 66, 337–345.
- [26] Ishaque, K., Salam, Z., (2013) 'A review of maximum power point tracking techniques of PV system for uniform insolation and partial shading condition', Renew. Sustain. Energy Rev. 19, 475–488.
- [27] Salas, V., Oli'as, E., Barrado, A., La'zaro, A., (2006) 'Review of the maximum power point tracking algorithms for stand-alone photovoltaic systems', Sol. Energy Mater. Sol. Cells 90 (11), 1555–1578.
- [28] Mamarelis, E., Petrone, G., Spagnuolo, G., (2014) 'A two-steps algorithm improving the P&O steady state MPPT efficiency', Appl. Energy 113, 414–421.
- [29] Makhoulouf, M., Messai, F., Benalla H. (2012) 'Modeling and simulation of grid-connected hybrid photovoltaic/battery distributed generation system', Canadian Journal on Electrical and Electronics Engineering Vol. 3, No. 1, January 2012.
- [30] RezaReisi, A., Moradi, M.H., Jamasb, S. (2013) 'Classification and comparison of maximum power point tracking techniques for photovoltaic system: a review', Renewable Sustainable Energy Reviews Vol.:19, pp: 433–443.
- [31] Berrera, M., Dolara, A., Leva, S. (2009) 'Experimental test of seven widely adopted MPPT algorithms', IEEE Bucharest Power Tech Conference', June 28th – July 2nd, Bucharest, Romania.
- [32] Femia, N.; Petrone, G.; Spagnuolo, G.; Vitelli, M.,(2004) 'Perturb and observe MPPT technique robustness improved', IEEE International Symposium on Industrial Electronics, vol.2, pp. 845- 850, May 2004.
- [33] Kamel, R.M., Chaouachi, A., Nagasaka, K. (2009) 'Design and implementation of various inverter controls to interface distributed generators (DGs) in micro grids' Conference on Energy System, Economy and Environment, Tokyo, pp. 60-64.
- [34] Houssamo, I., Locment, F., Sechilariu, M. (2013) 'Experimental analysis of impact of MPPT methods on energy efficiency for photovoltaic power systems', International Journal of Electrical Power & Energy Systems, Volume 46, March 2013, pp:98–107.
- [35] Radjai, T., Rahmani, L., Mekhilef, L., Gaubert, J.P. (2014) 'Implementation of a modified incremental conductance MPPT algorithm with direct control based on a fuzzy duty cycle change estimator using Dspace', Solar Energy Vol.:110, pp:325–337.
- [36] Altas, I.H., Sharaf, A.M. (2008) 'A novel maximum power fuzzy logic controller for photovoltaic solar energy systems', Renewable Energy, vol. 33, no.3, 2008, pp. 388-399.
- [37] Timothy, Ross, J. (2004) 'Fuzzy Logic with Engineering Applications' second ed. John Wiley & Sons Ltd.